MATHIMATICAL MODEL TO PREDICT THE DESIGN AND PERFORMANCE OF HIGH-SPEED TURBOPUMPS

Mr. Ali Ahmed Gitan
Mech. Eng. Dept.
Collage of Engineering
University of Baghdad

Prof. Dr. Najdat N. Abdulla
Mech. Eng. Dept.
Collage of Engineering
University of Baghdad

Dr. Abdul Kareem A. Al-Doori
Mech. Eng. Dept.
Collage of Engineering
University of Baghdad

ABSTRUCT

In this work a high-speed turbopumps of (22000 rpm) rotational speed, which are oxidizer and fuel turbopumps, are designed. The design requirement for mass flow rate and outlet pressure are (12.5 kg/s) and (113×10^5 Pa) respectively for the oxidizer turbopump, and (3.5 kg/s) and (95×10^5 Pa) respectively for the fuel turbopump. The design work of centrifugal pump is divided into impeller and volute design works. The impeller design work is performed by the streamline curvature and quasi-orthogonal technique based on hub-to-shroud mean stream surface between two blades with assistance of experimental design coefficients and relations for first prediction. The volute is designed by using the method of constant angular momentum, where in this method the tangential and radial velocities are considered uniform around the impeller. The numerical results are compared with experimental data of the actual pumps, and it is found that these results agree well with the real designs. The output of the design program is used as an input to the performance program. The performance prediction is achieved by three dimensional, steady, incompressible and viscous flow analyses through the blade passage. The ANSYS program has been employed to solve these equation in order to predict the flow characteristics at design and off-design conditions. The analysis is done at many operation conditions, which have the range of flow coefficient ratio (Φ/Φ_m) from (0.4) to (1.8), and the results are compared with experimental results for previous work to make sure the validity of the analysis program at design and off-design conditions.

الخلاصة

في هذا العمل تم تصميم مضخات توربينية ذات سرع عالية و هن مضخات المؤكسد و الوقود بسرعة دورانية (22000 دورة/دقيقة). إن متطلبات التصميم لمعدل الجريان الكتلي و الضغط الخارج هي (12.5كغم/ثا) و(113×10^5 باسكال) على التوالي لمضخة المؤكسد التوربينية، و (3.5 كغم/ثا) و (95×10^5 باسكال) على التوالي لمضخة الوقود التوربينية. إن عمل التصميم للمضخة الطاردة المركزية يقسم إلى تصميم البشارة و المجرى الحلزوني. إن عمل تصميم البشارة قد تم باستخدام تقنية تقوس خطوط الانسياب و أشباه الأعمدة و المستندة على متوسط سطح انسياب قاعدة الريشة – حافتها بين ريشتين بمساعدة معاملات التصميم و علاقات عملية لأول تنبؤ. لقد تم تصميم المجرى الحلزوني باستخدام طريقة الزخم الزاوي الثابت، حيث إن هذه الطريقة تفرض توزيع مركبتا السرعة المماسية و الشعاعية بصورة منتظمة حول البشارة. لقد تم مقارنة النتائج مع النتائج العملية لمضخات حقيقية، و وُجِد إن هذه النتائج تتوافق

بصورة جيدة مع التصاميم الحقيقية. إن البيانات الخارجة من برنامج التصميم قد استعملت كبيانات داخلة إلى برنامج الأداء. لقد أنجز التنبؤ بالأداء بتحليل جريان ثلاثي الأبعاد، مستقر، لا انضغاطي و لزج خلال مجرى الريشة. لقد تم توضيف برنامج ANSYS لحل تلك المعادلات من أجل التنبؤ بخواص الجريان عند الظروف التصميمية و الغير تصميمية. لقد تم التحليل عند عدة ظروف تشغيلية محددة بمدى نسبة معامل الجريان (Φ/Φ_m) من (0.4) إلى (1.8)، و قد قورنت النتائج مع نتائج عملية لعمل سابق للتأكد من صحة برنامج التحليل عند الظروف التصميمية و غير التصميمية.

KEY WORDS
Turbopump, Centrifugal pump, Turbopump design, High-speed turbopump, Centrifugal pump performance, Propellant pumps

INTRODUCTION

The trend toward higher process pressures, which has developed over the past half century or so, has provided impetus to exploit the advantages of high speed to better provide high head capability in centrifugal pumps. High head centrifugal design may be provided by using high rotating speed, by series multi-staging, or by a combination of both.

The characteristics of high-speed design are several as follows:

1- Fewer and smaller stages are required to meet a given head objective, and not infrequently, single–stage designs can provide capability that would otherwise require multi-staging.
2- Smaller, more compact design tends toward shorter shaft spans that can result in lower shaft deflection and improved shaft dynamics.
3- Compactness, involving fewer and smaller components, is economical of materials are required for handling severe process fluids.
4- Minimal spares inventory and relatively quick and easy maintenance are attributes of high speed, which are often very attractive to users, to whom pump availability of their businesses.
5- Lightened pump weight can translate into smaller and less expensive mounting foundations.

When the pump is driven by a turbine, the combined system is called a turbopump system. The supply of propellants to the inlet of the pumps at required minimum pressure is customarily considered the responsibility of the vehicle propellant system and thus of the vehicle designer. The main function of the turbopump feed system then is to rise the pressure of the propellants received from the vehicle tanks and deliver then to the main thrust chamber, through ducts and valves, at pressure and flow rates commensurate with rated engine operation. Because of its specific needs, the rocket industry has developed its own pump design approaches, which may differ from those for conventional applications. In addition, designers may employ their individual methods of analysis and calculation. However, the broad underlying principles are quite similar.

There are set of hydraulic pump design requirements that must be met in any design method:

1- Attain optimum efficiency
2- Obtain a stable total head, versus flow rate characteristic over the full operating range.
3- Minimize net positive suction head (NPSH) required for maintaining no cavitation.
4- Minimize the weight, cost and hydraulic size of pump, e.g., diameter of impeller.
5- Minimize hydraulically generated axial and radial thrust loads, the vibration and noise emission.

METHOD OF IMPELLER DESIGN

When more is known about the actual channel flow, it may be possible to design a blade shape and hence channels shape to obtain the optimum result.

The design method is an optimization method, which bases on the relationships between the experimental data of impeller and imperical approximations and the flow that adjust the calculation of geometry to be suitable with good flow characteristics.

Impeller Design Elements Calculations

From the Euler energy transfer equation of the pump the peripheral velocity at inlet is determined

$$U_2 = \sqrt{\frac{gH}{k_n \eta_h (1 - q_P)}} \tag{1}$$

The experimental test data gave a range values for k_n, η_h, and q_P, where k_n = 0.8 - 0.85, η_h = 0.8 - 0.85, and q_P = 0.05 - 0.1. The outlet diameter of the impeller can be calculated as:

$$D_2 = \frac{60U_2}{\pi N} \tag{2}$$

Eye diameter (D_e) must be designed for optimum *NPSH* and best cavitation performance, based on experimental data and empirical approximation [Salisbury 1983] as follows:

$$D_e = 4.66(Q/N)^{1/3} \tag{3}$$

The extent of prerotation can be specified by the ratio of the pitch per second (p_{1s}) to the inlet meridional velocity (V_{m1}). A forced vortex pattern of flow is assumed in the impeller approach. This ratio varies within narrow limits [Stepanoff 1957]

$$ratio = \frac{p_{1s}}{V_{m1}} = 1.15 - 1.25 \tag{4}$$

After the above correction, the inlet blade angle is calculated by the inlet velocity triangle relations

$$\beta_1' = \tan^{-1} \frac{p_{1s}}{U_1} \tag{5}$$

Another design coefficient can be defined which is the flow coefficient (Φ)

$$\Phi = \frac{V_{m2}}{U_2} \tag{6}$$

The flow coefficient for low specific speed high-speed engine pumps has a value in the range of (0.01 - 0.15) [Huzel and Huang 1967]. The experimental test data gives this variation value as a ratio of outlet to inlet relative velocities.

$$\overline{W} = \frac{W_2}{W_1} = \frac{A_1}{A_2} = \frac{D_1 b_1 \sin \beta_1'}{D_2 b_2 \sin \beta_2'} = 0.7 - 1 \tag{7}$$

The outlet width of the blade b_2 can be obtained by:

$$b_2 = \frac{D_1 b_1 \sin \beta_1'}{\overline{W} D_2 \sin \beta_2'} \tag{8}$$

Using an expression for account parameter of an impeller

$$q_P = \frac{V_{m2}}{U_2 \tan \beta_2'} = \frac{Q}{\pi D_2 b_2 U_2 \tan \beta_2'} \tag{9}$$

From the last equation, it can be show that

$$b_2 = \frac{Q}{\pi D_2 q_P U_2 \tan \beta_2'} \tag{10}$$

By equating eq. (7) and (9) the formula for definition of a blade angle on output can be obtained

$$\beta_2' = \cos^{-1} \frac{\pi U_2 D_1 b_1 q_P \sin \beta_1'}{\overline{W} Q} \tag{11}$$

The calculation values of inlet meridional velocity V_{m1} and inlet impeller diameter D_1 determine the width of the blade at inlet b_1. By the continuity equation with consideration of blockage area due to blade thickness

$$b_1 = \frac{Q_t}{(\pi D_1 - \frac{nt_1}{\sin \beta_1'}) V_{m1}} \tag{12}$$

$$b_2 = \frac{Q_t}{(\pi D_2 - \frac{nt_2}{\sin \beta_2'}) V_{m2}} \tag{13}$$

The number of blade n is determined for optimum efficiency and a thinner edge at inlet is assumed (typical value is 3mm) and this results in better efficiency if the angle β_1' has the correct value.

Through Flow Analysis

The flow distribution is calculated by solving an equation for the directional derivative of the relative velocity along the quasi-orthogonals in the meridional plane. The derivation of equation is presented in reference [Al-Hamdani 1993]. The final form is given as follows:

$$\frac{dw}{ds} = \left[A \frac{dr}{ds} + B \frac{dz}{ds} \right] W + C \frac{dr}{ds} + D \frac{dz}{ds} - \left[E \frac{dr}{ds} + F \frac{dz}{ds} \right] \frac{1}{W} \tag{14}$$

where:

$$A=\frac{\cos(\alpha)\sin^2(\beta)}{r_c}-\frac{\cos^2(\beta)}{R}+\sin(\alpha)\sin(\beta)\cos(\beta)\left(\frac{\partial\phi}{\partial R}\right)_f$$

$$B=-\frac{\cos(\alpha)\sin^2(\beta)}{r_c}+\sin(\alpha)\sin(\beta)\cos(\beta)\left(\frac{\partial\phi}{\partial z}\right)_f$$

$$C=\sin(\alpha)\sin(\beta)\frac{dW_m}{dm}-2\omega\cos(\beta)+R\sin(\beta)\left[\frac{dW_\phi}{dm}+2\omega\sin(\alpha)\right]\left(\frac{\partial\phi}{\partial R}\right)_f$$

$$D=\cos(\alpha)\sin(\beta)\frac{dW_m}{dm}+R\sin(\beta)\left[\frac{dW_\phi}{dm}+2\omega\sin(\alpha)\right]\left(\frac{\partial\phi}{\partial z}\right)_f$$

$$E=\frac{1}{\rho}\frac{\partial}{\partial R}\left[2\mu_{eff}\frac{\partial W_r}{\partial R}\right]+\frac{1}{\rho}\frac{\partial}{\partial z}(\tau_{zr})+\frac{2\mu_{eff}}{\rho R}\left[\frac{\partial W_r}{\partial R}-\frac{W_r}{R}\right]+\left[\frac{R}{\rho}\frac{\partial}{\partial z}(\tau_{z\phi})+\frac{R}{\rho}\frac{\partial}{\partial R}(\tau_{r\phi})+\frac{2}{\rho}(\tau_{r\phi})\right]\left(\frac{\partial\phi}{\partial R}\right)$$

$$F=\frac{1}{\rho}\frac{\partial}{\partial z}\left[2\mu_{eff}\frac{\partial W_z}{\partial z}\right]+\frac{1}{\rho R}\frac{\partial}{\partial R}(R\tau_{rz})+\left[\frac{R}{\rho}\frac{\partial}{\partial z}(\tau_{z\phi})+\frac{z}{\rho}(\tau_{r\phi})+\frac{2}{\rho}(\tau_{r\phi})\right]\left(\frac{\partial\phi}{\partial z}\right)$$

The coordinate system and the rotation axis are shown in **Fig. (1)**. In addition to eq. (14), the continuity equation must be satisfied from hub-to-shroud. This is done by solving eq. (14) simultaneously with the continuity equation in its integral form along each quasi-orthogonal. The form of the continuity equation used is as follows:

$$\dot{m}=n\int_0^s\rho W_n R\xi ds \tag{16}$$

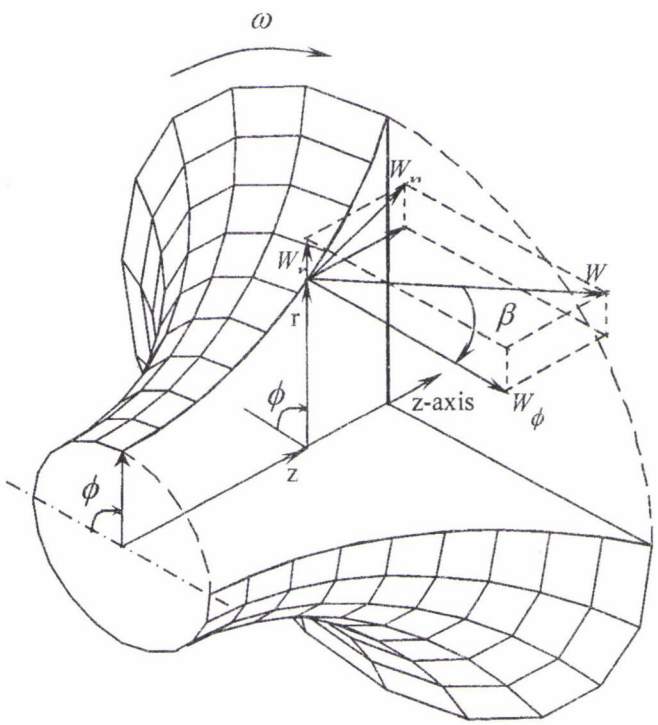

Fig. (1) Coordinate system and velocity component

The pressure along streamline can be calculated from the Bernoulli equation for rotating parts.

$$P+\frac{\rho W}{2}-\frac{\rho(R\omega)^2}{2}=C \tag{17}$$

Viscous Terms Calculations

In order to determine the turbulent viscosity, an algebraic model based on modified Prandtl's mixing length theory was chosen to be used in the present work [Abu-Tabikh 1990]. The turbulent contribution to the effective viscosity is then calculated from the following relation:

$$\mu_{turbulent}=\rho l_m^{\,2}\left[\left(\frac{\partial W_y}{\partial y}\right)^2+\left(\frac{\partial W_\phi}{\partial y}\right)^2\right]^{1/2} \tag{18}$$

Friction Losses Calculation

The must obvious loss of head in the impeller is due to frictional losses similar to those encountered in any flow within a conduit. Boundary layers and separated flow regions occur which dissipate kinetic energy in the flow. The friction flow losses are usually computed from the equation

$$H_f=f\frac{L}{D}\frac{W^2}{2g} \tag{19}$$

The Slip of Flow

A slip factor σ may be defined as the tangential components of absolute velocity corresponding to the outlet mean flow angle β_2 to the same velocity corresponding to the outlet blade angle β_2' [Dixon 1975]. Many attempts at predicting the amount of slip from impellers have been made. Wiesner [Wiesner 1967] made a review of various methods, which have been proposed for the estimation of basic slip factors for centrifugal impellers. He then presents a very simple empirical expression, which fits the Busemann results extremely well over the whole range of practical blade angles and number of blades up to limiting inlet-to-outlet radius ratio for the impeller. An empirical correction factor is also proposed for conditions, which exceed this limiting radius ratio. The limiting radius ratio that presented by Sheet [Sheet 1950] and employed by Wiesner is given as

$$\ln\left(\frac{R_2}{R_1}\right)_{max}\cong\frac{1.30\cdot 2\pi\sin\beta_2'}{n}\cong\frac{8.16\sin\beta_2'}{n} \tag{20}$$

In general, the test slip coefficients can be seen to correlate very well with the basic slip factors as specified by Busemann, and it has been found that these, in turn, can be very closely expressed by the simple empirical function:

$$\sigma=1-\frac{\sqrt{\sin\beta_2'}}{n^{0.07}} \tag{21}$$

This relation is taken to be applicable up to the limit of blade solidity based on eq. (20):

$$\epsilon_{limit} = \frac{R_1}{R_2} \cong \frac{1}{\ln^{-1} \frac{8.16 \sin \beta_2'}{n}} \tag{22}$$

For impeller mean radius ratios in excess of this limit, the following equation has been found to be fair agreement with the Busemann slip factor in these areas:

$$\sigma = \left(1 - \frac{\sqrt{\sin \beta_2'}}{n^{0.07}}\right)\left[1 - \left(\frac{\frac{R_1}{R_2} - \epsilon_{limit}}{1 - \epsilon_{limit}}\right)^3\right] \tag{23}$$

The Consideration of Cavitation

To avoid cavitation during operation of a propellant pump, the pump-inlet available net positive suction head $(NPSH)_a$ furnished by the propellant feed system upstream of the pump, must be higher than the suction head above the propellant vapour pressure at which cavitation would set in. $(NPSH)_a$ is the difference between the propellant inlet total pressure head and the propellant vapour pressure.

$$(NPSH)_a = \frac{P_1}{\rho g} - \frac{P_v}{\rho g} \tag{24}$$

In design practice the term "critical net positive suction head", or $(NPSH)_c$, is used to indicate the minimum suction head required above the propellant vapour pressure to assure suppression of cavitation. For critical operation, a good empirical relation that gives an acceptable operation $(NPSH)_c$ for modern industrial designs is presented by Salisbury [Salisbury 1983]. This relation is given as follows:

$$(NPSH)_c = 0.001046 N^{4/3} Q^{2/3} \tag{25}$$

The above two eq. (24) and (25) give the value of inlet pressure to the impeller P_1, which is used in the determination of local pressure along streamline by using eq. (17).

METHOD OF VOLUTE DESIGN

The flow in the volute has very nearly the spiral flow. The local value of the average velocity follows the angular momentum equation, so that [Lorett and Gopalakrishnan 1986]:

$$RV_{\phi v} = R_2 V_{\phi 2} = C \tag{26}$$

If friction is neglected, the flow through the differential section shown in **Fig. (2)** is

$$dQ_{\phi v} = dAV_{\phi v} = bdRV_{\phi v} \tag{27}$$

But $V_{\phi v} = C / R$, hence $dQ = bdRC / R$, and the total flow past the section becomes

$$Q_{\phi v} = \int_{R_2}^{R_{\phi v}} dQ = C \int_{R_2}^{R_{\phi v}} \frac{b\,dR}{R} \tag{28}$$

Substituting for $Q_{\phi v}$ the term $\phi v Q/360$ results

$$\phi v^{o} = \frac{360C}{Q} \int_{R_2}^{R_{\phi v}} b \frac{dR}{R} = \frac{360 R_2 V_{\phi v 2}}{Q} \int_{R_2}^{R_{\phi v}} b \frac{dR}{R} \tag{29}$$

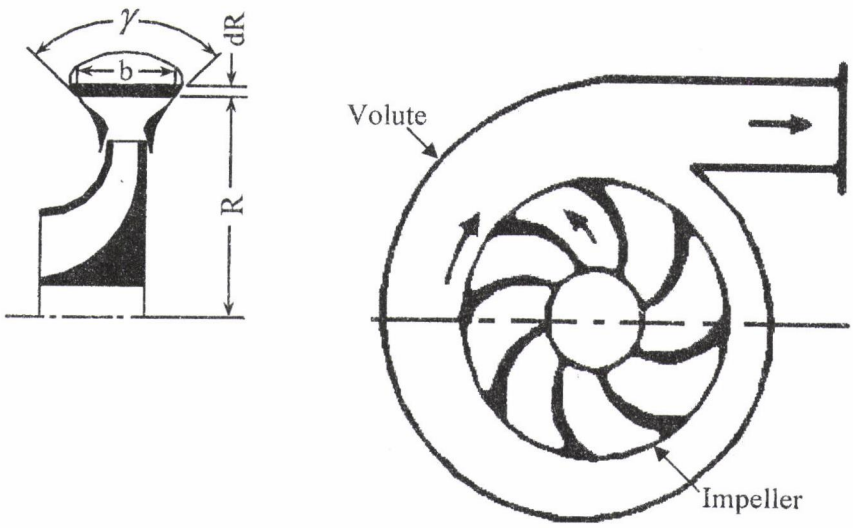

Fig. (2) Section through volute

In order to simplify the calculations it may be assumed that the top of the volute is parallel to the shaft axis. The width of the volute at any point (b) may be calculated by the equation

$$b = b_3 + 2(R - R_2)\tan\left(\frac{\gamma}{2}\right) \tag{30}$$

Substituting eq. (30) into eq. (29) and solving the integration yields

$$\phi v^{o} = \frac{360 R_2 V_{\phi 2}}{Q}\left\{\left[\left(b_3 - 2R_2\tan\frac{\gamma}{2}\right)\ln R_{\phi v} + 2R_{\phi v}\tan\frac{\gamma}{2}\right] - \left[\left(b_3 - 2R_2\tan\frac{\gamma}{2}\right)\ln R_2 + 2R_2\tan\frac{\gamma}{2}\right]\right\} \tag{31}$$

To calculate the volute areas, trapezoidal area rule can be used according to the shape of the volute section area.

$$A_{\phi v} = \frac{(R_{\phi v} - R_2)(b_3 + b_{\phi v})}{2} \tag{32}$$

The discharge velocity from the nozzle (V_{noz2}) for high-speed rocket engine pump application has a ranged value of (15-30 m/s). From this velocity specification the outlet area of the nozzle can be calculated.

$$A_{noz2} = \frac{Q}{V_{noz2}} \tag{33}$$

The nozzle has a circular cross section area, hence the diameter of the discharge area (D_{noz2}) can be calculated. Usually the angle of nozzle divergence (λ) has a range of (6^{o}-12^{o}) for efficient loss coefficient. Length of the nozzle (L_{noz}) is determined by equivalent angle of nozzle divergence (λ).

$$L_{noz} = \frac{D_{noz2} - D_{t}}{2\tan\left(\frac{\lambda}{2}\right)} \tag{34}$$

FLOW ANALYSIS WORK FOR PERFORMANCE PURPOSE

The performance of the pump can be predicted by obtaining a characteristic head-versus-capacity curve. It is necessary to get this characteristic curve for any pump to make sure that this pump works in the safe range of capacity and doesn't reach the operation limits that are known by surging. In the present work and for new design problem the theoretical analysis could be followed by solving set of differential equations numerically by using the ANSYS 5.4 package. The mathematical formulation of this problem is governed by basic conservation principles of both mass and momentum.

ANSYS Method

The fluid flow problem is defined by the laws of conservation of mass, momentum, and energy. These laws are expressed in terms of partial differential equations, which are discretized with a finite element based technique in ANSYS program. The ANSYS computer program is a large-scale general-purpose finite element program, which may be used for solving several classes of engineering problems. There are some assumptions and restrictions are selected to describe the present problem with possible simplest form, those are:

1- The problem domain and the finite element mesh that shown in **Fig. (3)** may not change during the analysis.
2- The fluid is single-phase fluid.
3- The flow is assumed three-dimensional, incompressible, steady, turbulent and adiabatic flow.
4- The turbulent model used is k-ε model.
5- The boundary conditions are as follows:

a- At wall surfaces the wall surfaces are represented by blades, hub and shroud surfaces, where the velocity is set equal to zero on this surface because of viscosity effect, and this can be lead to the pressure at the wall is set equal to that at the nearest point to the wall.
b- At inlet velocities are prescribed at inlet, where w-component is prescribed equal the velocity entering the impeller, u-component is set equal to $-\omega r$ (i.e. the flow is assumed axial in fixed coordinates), and v is set equal to zero.
c- At exit a smooth exit has been assumed, i.e. the second partial derivative of the three components of exit velocity is set equal to zero.

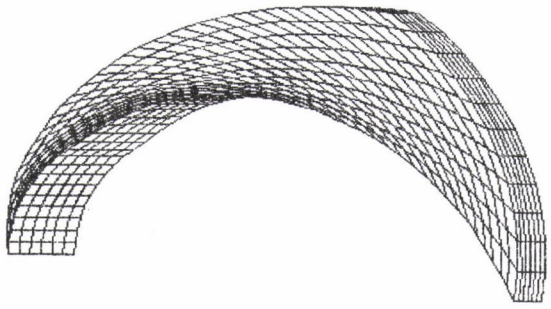

Fig. (3) Three-dimensional mesh used by ANSYS program

DESIGN WORK RESULTS

The method used in designing the high-speed centrifugal pump is applied to the three kinds of centrifugal pumps as mentioned in the last section. **Table (1)** shows the pertinent data for the cases under consideration.

Murakami Impeller

The first pump that has been redesigned by the present method is that described by Murakami [Murakami 1980]. Murakami described the pump impeller geometry only and no volute description is presented, therefore only the impeller has been considered for this pump. Large similarity between the blade geometry in Murakami impeller and the redesigned one obtained by the present are shown in **Fig. (4)**. Also, the overall design parameters show a good identity. The inlet radius has a little deviation from the original geometry. Indeed, the criteria that is always considered in the design of suction region is to keep the flow velocity as small as possible to prevent the cavitation phenomena. This may be accomplished by design the impeller inlet area as large as possible. In the other hand, the increase of the inlet blade radius increases the ability of impeller suction but it may cause cavitation in the region of the blade edge because of the high rotational speed of the blade. Therefore, the inlet blade radius must be adjusted with corrections based on experimental results to get the proper design. The shroud profile of the original blade has a small radius of curvature in the inlet region followed by straight shroud edge, and this profile may be cause a wake losses in the outlet region of the passage. In the other hand, the resulting profile of the redesigned impeller shroud has a uniform curvature and gradual change in direction from axial to radial direction; therefore this reduces the possibility of separation and wake occurrence.

The blade-to-blade mean surface has been computed too, and their result has been represented by **Fig. (5)**. The comparison of blade angles between the original and present works is remarked in **Table (2)**, where it shows a good agreement in spite of the simple difference in the inlet blade angle. The difference that is noticed in the inlet blade angle was resulted from the assumption of uniform inlet flow velocity, which may be increased because of the blockage happened by the recirculation effect that is causing an increment in the inlet blade angle value.

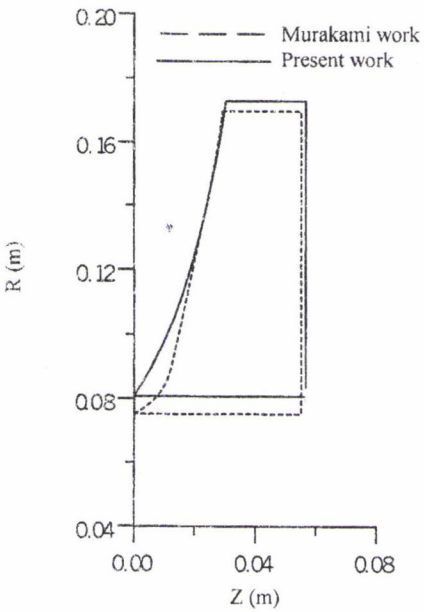

Fig. (4) Impeller blade profile for Murakami pump and redesign pump

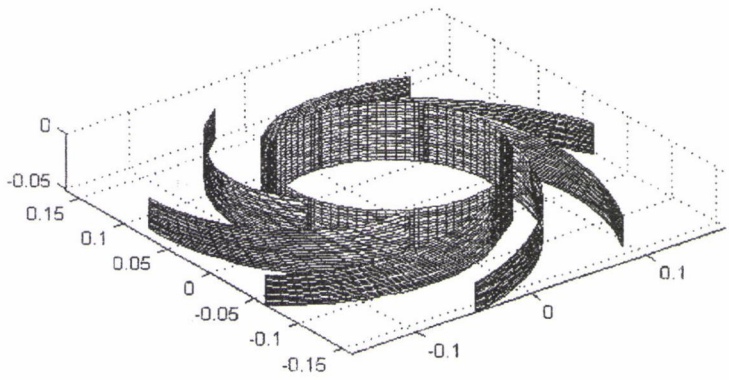

Fig. (5) The redesigned impeller of Murakami pump

Table (1) The pertinent data for the cases under consideration

Pump Type	Murakami Pump	Oxidizer Pump	Fuel Pump
Rotational speed (rpm)	400	22000	22000
Mass flow rate (kg/s)	18.85	12.5	3.5
ΔP (Pa$\times 10^5$)	0.19318	113	95
Blade thickness (mm)	10	3	3
Density (kg/m^3)	1000	1600	800
Viscosity (Pa.s)	0.00106	0.000672	0.000336

Table (2) Blade angles of the original design and present design

Pump Type	Inlet Blade Angle (deg)			Outlet Blade Angle (deg)		
	Original work	Present work	Error %	Original work	Present work	Error %
Murakami Pump	22.33	19.03	14.7	27	28.49	5.5
Oxidizer Pump	19	16.62	12.5	28	28.36	1.28
Fuel Pump	21	16.79	20	32	28.95	9.5

Oxidizer Turbopump Impeller

The original blade geometry of Russian oxidizer turbopump and the redesigned blade for the present work is shown in **Fig. (6a)**. The results for inlet and outlet widths and inlet and outlet radii, which are obtained by the present method, have acceptable values comparing with those of original geometry. The difference that is obtained in the redesigned geometry can be remarked in the inlet region, where the radius of the inlet blade edge has been assumed constant for simplicity. The same

result that was obtained by the previous pump for the blade angles was obtained here, where the values of blade angles for the present design are less than that of the original type. The redesigned oxidizer impeller is shown by **Fig. (7)**, but **Table (2)** shows the blade angles values for the comparison.

Fuel Turbopump Impeller

The fuel pump of Russian rocket engine, which its pertinent data is shown in **Table (1)**, represents another type of high-speed turbopump that has been considered. The only difference between the previous type and the present one is that the fuel impeller has additional splitter blades. These blades are shorter than the main blades and the inlet radius is larger than that of the main blades but these have the same outlet radius, which is the outlet radius of the impeller. However, the addition of the splitter blades is used after a set of experimental tests for the impeller in order to reduce the slip losses. In the present work the splitter blades is not considered because there is no experimental data available, therefore some difference has been appeared in the redesigned geometry comparing with original geometry that contain splitter blades. **Fig. (6b)** shows a comparison between the real blade and the present work. A logical difference appears in the outlet blade width, where the redesigned blade width is less than that of the original blade due to the existence of the splitter blades in the original impeller. Therefore, the outlet flow area of the impeller has been reduced by an additional blade thickness, thus the blade width must be increased to keep the cross-sectional area of the radial flow path near constant as it must be done for most impellers in centrifugal pumps. In the other hand, the inlet width value of the redesigned blade didn't differ widely from that of the original blade because there are no splitter blades in both cases, where the splitter blades starts with a radius larger than that of the main blades. Due to the difference in the outlet blade width the shroud profile was shifted, but its properties stay as good as that of the profiles in the previous cases. The blade angles obtained for this pump impeller show reasonable agreement in the outlet. The deviation in the value due to existence of split blades, which are not considered, while the large error in the inlet blade angle may be imputed to the uniform inlet velocity assumption, which should be adjusted by an experimental test to the redesigned impeller.

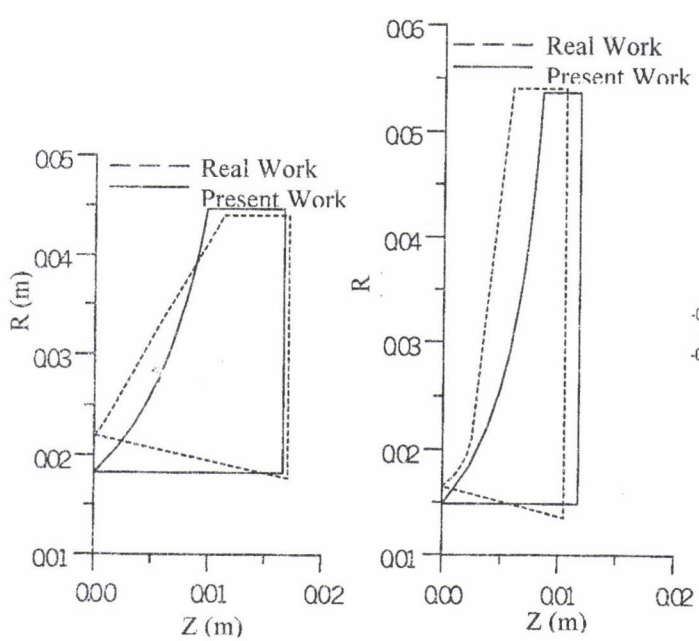

a. Oxidizer pump b. Fuel pump

Fig. (6) Impeller blade profile for real propellant pumps and their redesign pumps

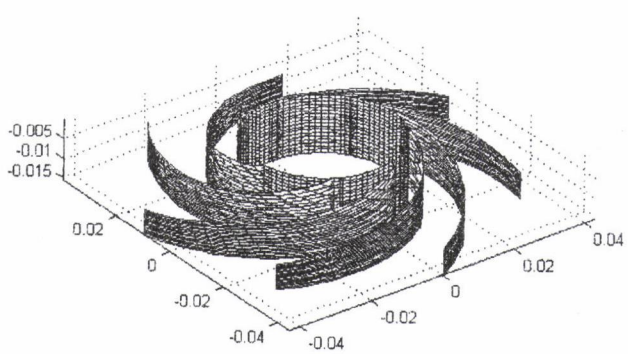

Fig. (7) The redesigned impeller of oxidizer pump

Volute Casing of Oxidizer Turbopump

A schematic plot for the volute casing designed by the present method is shown in **Fig. (8)**. **Fig. (8a)** shows an axial view for the volute, where the spiral passage and discharge nozzle are shown.

Fig. (8b) represents the sectional area shape of the volute, which represents an approximate shape for the typical shape shown by dashed line. Some of the design results for this volute are shown in **Table (3)**. In **Fig. (8a)**, the spiral part shows a small change in radius with angle changes because of the small angle of the absolute flow exit from the impeller with the periphery. This small angle is due to the high rotational speed of the impeller; therefore this volute shape is a geometric feature of the high-speed centrifugal pumps. For the same reason of small discharge angle from the impeller, a larger angle between the sides of spiral part may be used since the flow is then more nearly tangential. A smaller angle and larger radii give better results, but at the same time, the casing diameter and weight of the pump are increased unduly, therefore the maximum total angle of 60° between the sides is used, which is considered to be a suitable angle for this kinds of pumps as shown in **Fig. (8b)**. This figure represents a side view of the spiral part of the volute designed in the present work at many sections, where the dashed line represents the modification that can be done for the designed shape (solid line) with keeping the same area.

Table (3) Some design results for oxidizer turbopump volute

Design Element	Designed Value
Cutwater Diameter (m)	4.67453E-2
Tongue Angle (deg)	4.41924
Volute Width (m)	1.58515E-2
Discharge Nozzle Diameter (m)	1.28655E-2
Throat Area (m^2)	1.15519E-4

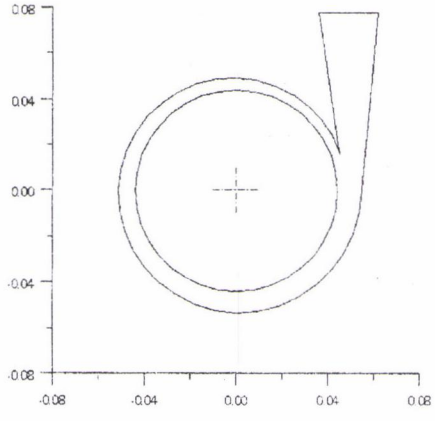

a) Axial view for the redesigned volute in meter unit

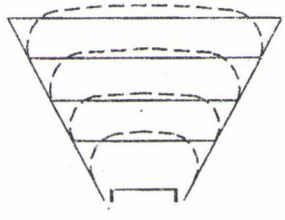

b) Side view for the redesigned volute

Fig. (8) The redesigned volute casing

FLOW ANALYSIS WORK RESULTS

Three dimensional theoretical analysis results of the flow between two blades have been done by using ANSYS program. Two types of impellers have been examined, low speed impeller represented by Murakami impeller and high-speed impeller represented by oxidizer turbopump impeller.

Murakami Impeller

The change of flow pattern along the impeller passage is shown in **Fig. (9)** and **Fig. (10)**. The flow velocity distribution along blade-to-blade distance in the midway between hub and shroud at flow coefficient ratio (Φ/Φ_m)=0.65 is shown in **Fig. (9a)** and **b**. **Fig. (9a)** shows the result at $r/r_2 = 0.7$, where the flow velocity in the low-pressure side (suction side) decreases but it is larger than that of experimental work. In the other hand the flow velocity in the high-pressure side (pressure side) has a difference between the experimental and present work less than that in the suction side. The velocity in the midway between suction and pressure side has a good result with the experimental work. There is many reasons cause the difference between the present work and experimental work. First, an approximate design is used in the analysis work because there is no information about the blade profile of the exact original geometry. Second, the flow analysis is done for the impeller only without any boundary condition that represents the volute effect; therefore the volute effect is negligible in the present analysis work. Third, no prerotation is assumed in the inlet boundary condition and the inlet radial velocity component is neglected. Forth, the pressure at the wall is assumed equal to that at the nearest point to the wall. Fifth, a unique passage between two blades is considered in this work without any neighboring passage effect representing by the difference in pressure in the blade tips. All of these reasons may cause a difference in results between the theoretical and experimental works. **Fig. (9b)** show the flow velocity distribution at exit of the impeller and it gives a good representation comparing with the experimental results, but there is some deviation in results near the wall. This difference can be imputed to the assumption of the equating pressure at the wall and the nearest point to the wall. The large difference near the suction side has been occurred because the fluid in the suction side region comes over the blade tip from the pressure side of the neighboring passage of experimental impeller.

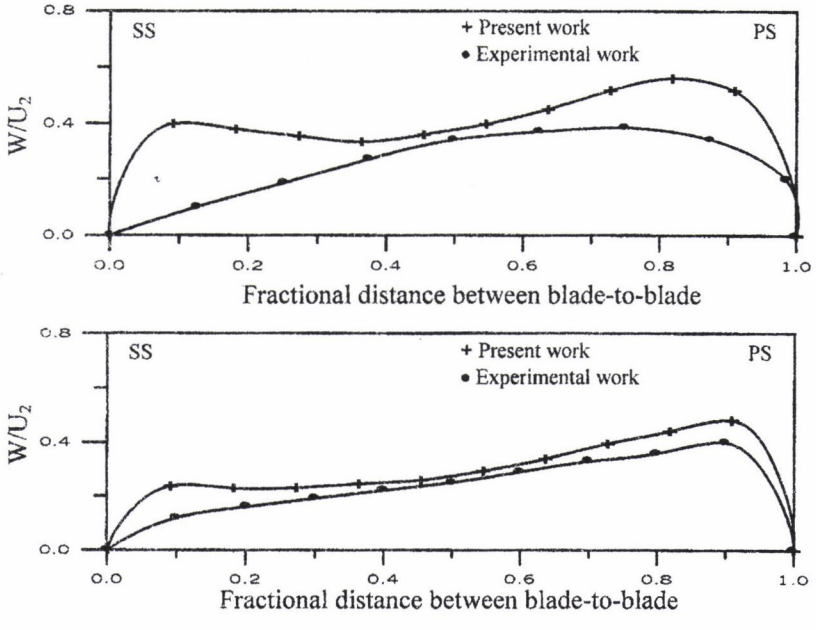

a) At $r/r_2 = 0.7$

b) At exit

Fig. (9) Relative velocity distribution along blade-to-blade distance in the midway between hub and shroud for Murakami pump at $(\Phi/\Phi_m) = 0.65$

Fig. (10a), **(b)** and **(c)** show the flow velocity distribution along blade-to-blade distance in the midway between hub and shroud at design condition where (Φ/Φ_m)=1.0. **Fig. (10a)** represents the results at the inlet to the blade passage, and it shows a very good representation for the flow velocity distribution comparing with experimental results. **Fig. (10b)** gives a good result except near the wall, where the velocity has a maximum value near the suction side and minimum value

near the pressure side and this is the same trend for that of experimental work. **Fig. (10c)** shows a uniform velocity profile, where the decreasing of velocity near the suction side in the experimental work is happened due to the pressure difference at the impeller tips.

The pressure distribution in the channel between two blades is shown in **Fig. (11)** and **(12)**, which represented as a pressure coefficient contour plotting. **Fig. (11a)** shows the contour lines drawn on the shroud surface when $(\Phi/\Phi_m)=0.65$ for the experimental work and **Fig. (11b)** represents the pressure contour when $(\Phi/\Phi_m)=0.65$ of the present work. The pressure contour of present work refers to the pressure increasing in the circumferential direction toward the pressure side, and there are some differences between this contour and that of **Fig. (11a)**. This due to first, the minus pressure which created near the inlet especially near the suction side in the present work and this is exactly the region where the cavitation is expected to occur. The main reason of this difference in results is that the inlet pressure has been assumed zero because there is no information about the inlet pressure or the suction pressure applied in the experimental work of Murakami. Second, the contour lines shown in **Fig. (11b)** have an inclination angle with the circumferential direction larger than that of **Fig. (11a)** especially near the suction side. The wake which occurred experimentally has been caused the increase of pressure near the suction side but this wake has less effect in the present work as it mentioned previously; therefore it leads to a less increase in pressure near the suction side of **Fig. (11b)**. Third, the pressure distribution shown in **Fig. (11b)** at the exit of channel is not uniform as in **Fig. (11a)** because of the absence of volute effect that cause uniform condition at the impeller exit. **Fig. (12)** represents the pressure distribution on the shroud surface between two blades when $(\Phi/\Phi_m)=1.0$.

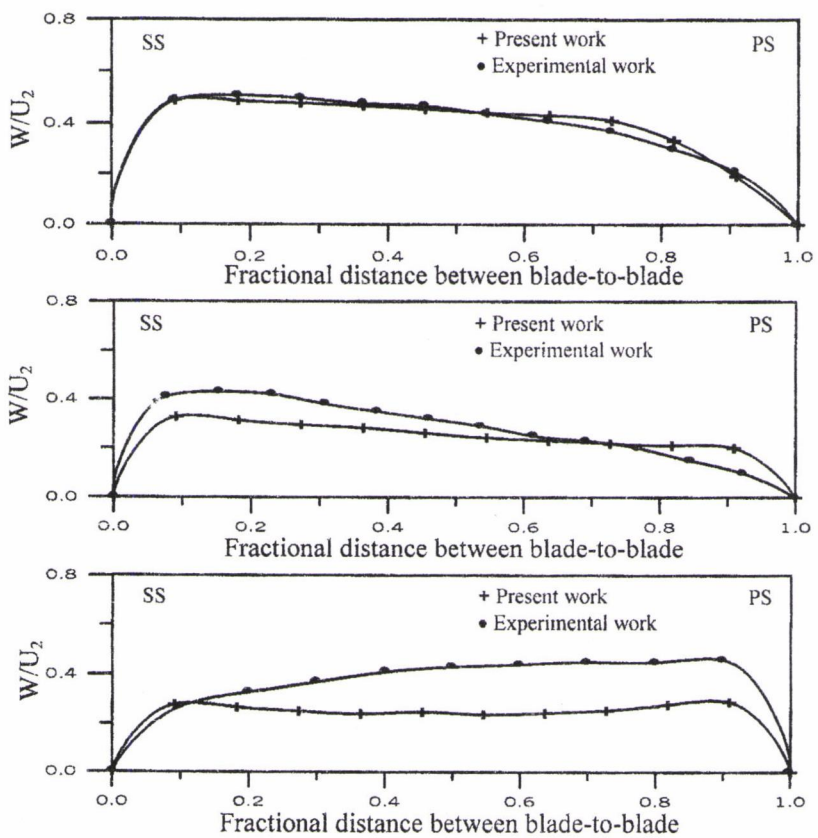

a) At inlet

b) At $r/r_2 = 0.7$

c) At exit

Fig. (10) Relative velocity distribution along blade-to-blade distance in the midway between hub and shroud for Murakami pump at $(\Phi/\Phi_m) = 1.0$

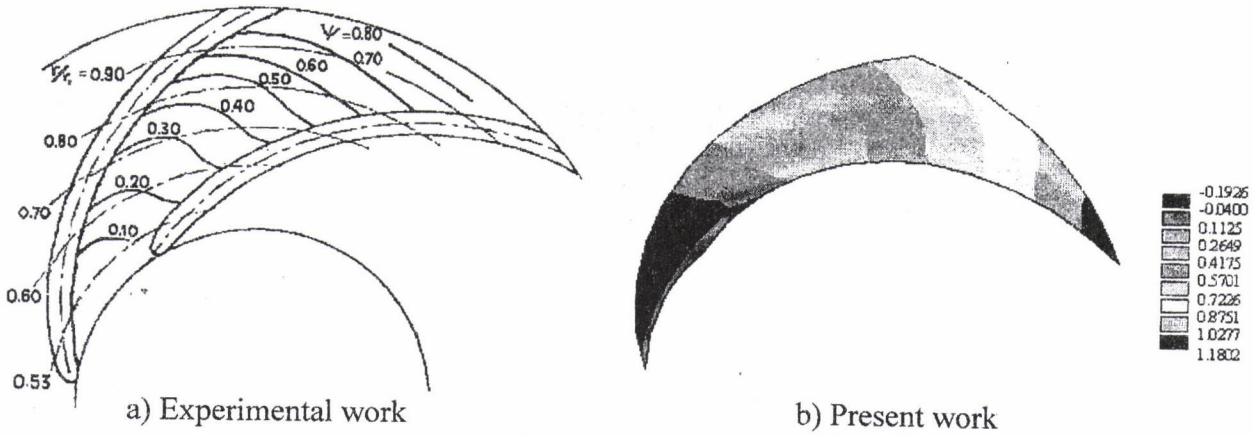

a) Experimental work b) Present work

Fig. (11) Pressure contour on the blade-to-blade surface for Murakami impeller at $(\Phi/\Phi_m) = 0.65$

circumferentially toward the pressure side and this is the same behavior that obtained by the present work as shown in **Fig. (12a)** and **(b)**. The same phenomena have been obtained at this flow rate as that happened in the off design flow rate except that there is no difference on the suction side and the contour lines have a simple difference in inclination angle due to the absence of the wake. An important result has been noticed from these figures, that the average pressure coefficient obtained by present work had the same value of the experimental work and this is the main aid of all process.

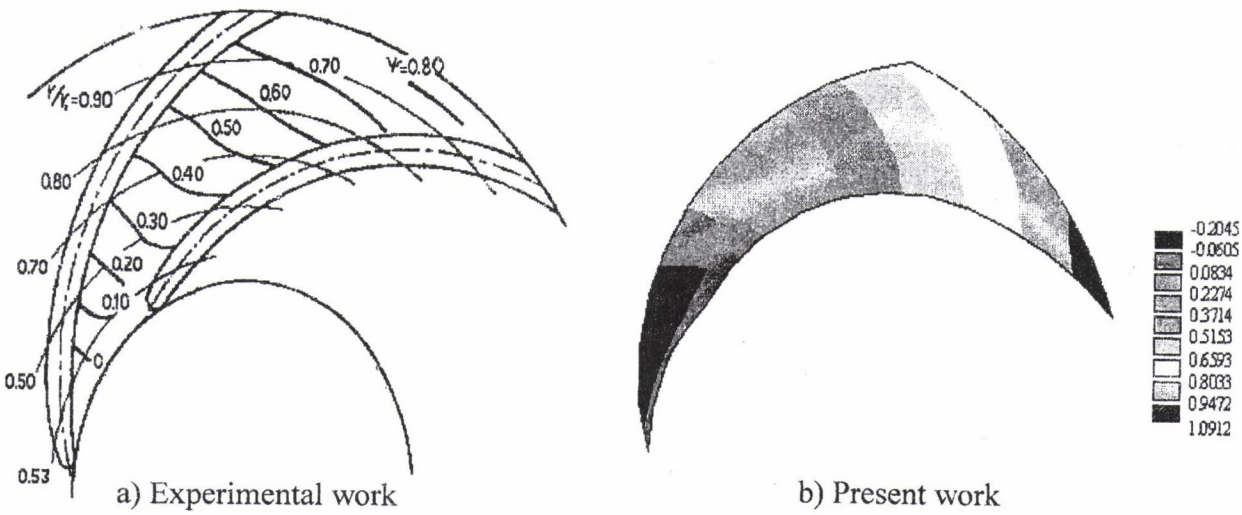

a) Experimental work b) Present work

Fig. (12) Pressure contour on the blade-to-blade surface for Murakami impeller at $(\Phi/\Phi_m) = 1.0$

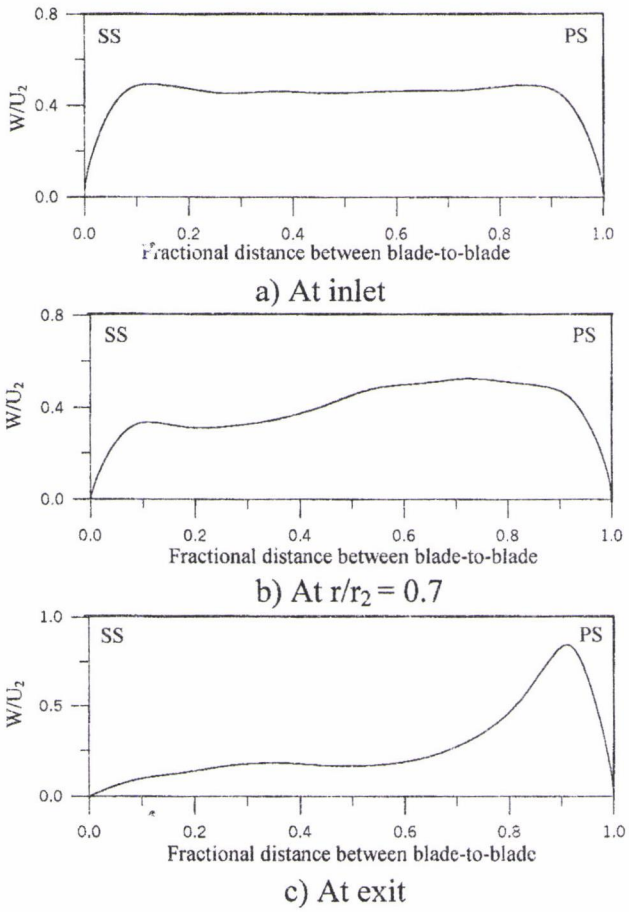

Fig. (13) Relative velocity distribution along blade-to-blade distance in the midway between hub and shroud for oxidizer pump at (Φ/Φ_m)=0.6

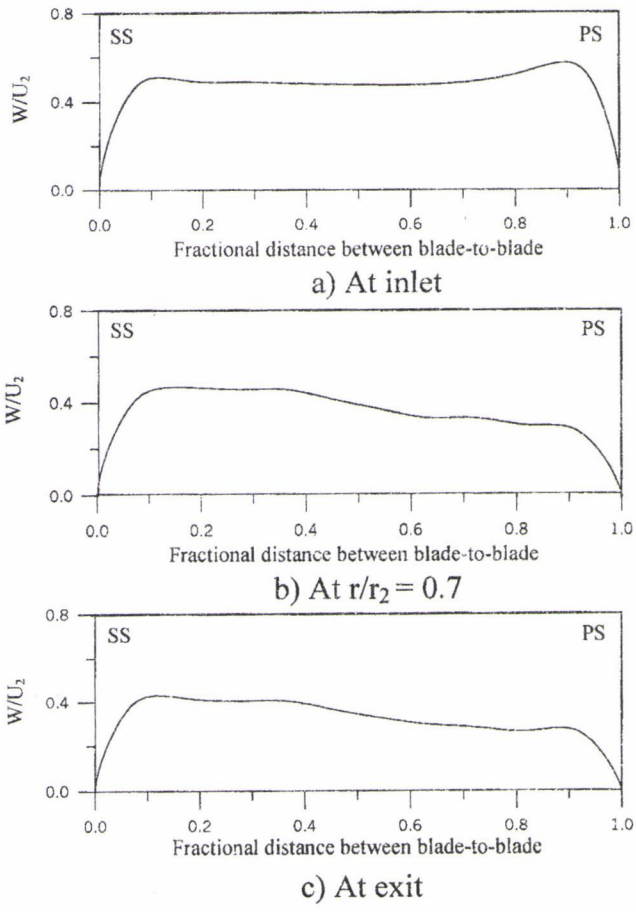

Fig. (14) Relative velocity distribution along blade-to-blade distance in the midway between hub and shroud for oxidizer pump at (Φ/Φ_m)=1.0

Oxidizer Turbopump Impeller

Fig. (13) represents the velocity distribution on blade-to-blade surface in the midway between hub and shroud at three positions when flow coefficient (Φ/Φ_m)=0.6. A uniform velocity distribution remarked at the inlet of impeller passage as shown in **Fig. (13a)**. At r/r_2 = 0.7 the velocity distribution is changed as shown in **Fig. (13b)**, where some reduction is occurred in velocity near the suction side and this behavior is observed in Murakami impeller with the difference in the shape of velocity profile. A remarkable difference is occurred in velocity levels between the suction and the pressure sides at exit of passage as shown in **Fig. (13c)** because of the reduction in velocity near the suction side and consequently the main flow will shift to the pressure side. **Fig. (14)** represents the velocity distribution on blade-to-blade surface in the midway between hub and shroud at three positions too when (Φ/Φ_m)=1.0. The velocity is uniformly distributed at the inlet of the passage as shown in **Fig. (14a)**, while a reduction in velocity occurred near the pressure side as shown in **Fig. (14b)** and a similar distribution is taken place at the exit as shown in **Fig. (14c)**. The flow pattern on the blade-to-blade surface in the midway between hub and shroud for the all domain from inlet to outlet of the passage is given as a velocity vector in **Fig. (15)**. The flow shows law velocity near the suction side and high velocity near the pressure side when (Φ/Φ_m)=0.4 and 0.6 as shown in **Fig. (15a)** and **b** respectively. When (Φ/Φ_m)=1.0 the velocity is reduced near the pressure side and velocity is increased near the wall at the inlet because of blade edge effect as shown in **Fig. (15c)**. The same behavior is remarked when (Φ/Φ_m)=1.0 with a little increasing in flow velocity at the suction side of the inlet region as shown in **Fig. (15d)**. A remarkable change in flow

pattern is resulted when (Φ/Φ_m)=1.6, where a deviation in flow is obtained at the exit of the passage near the suction side toward the pressure side, which cause a reduction in the exit flow area. Consequently the fluid leaves the passage with very high velocity levels near the pressure side as shown in **Fig. (15e)**. The same behavior is occurred when (Φ/Φ_m)=1.8 as shown in **Fig. (15f)**.

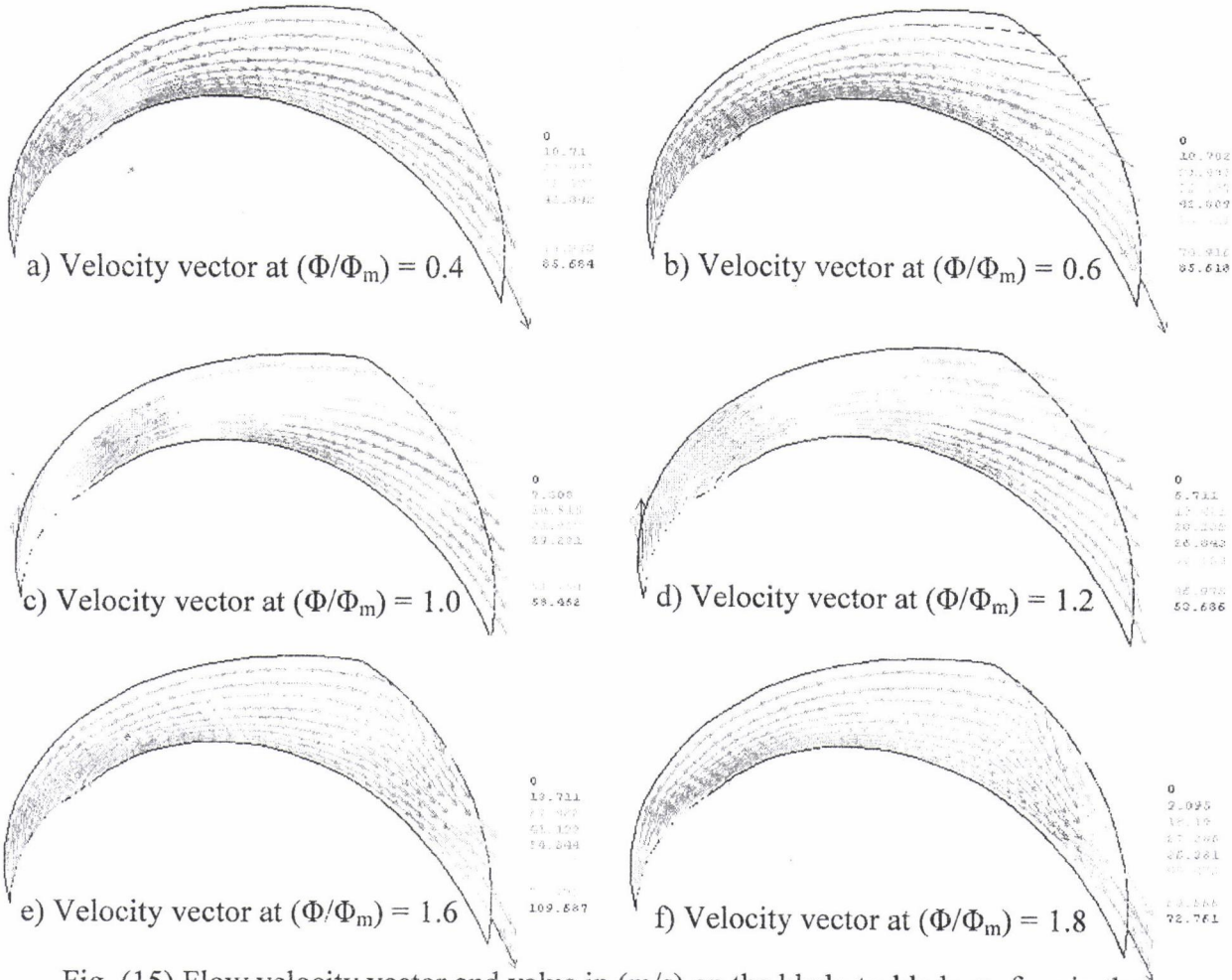

Fig. (15) Flow velocity vector and value in (m/s) on the blade-to-blade surface in the midway between hub and shroud for oxidizer pump impeller

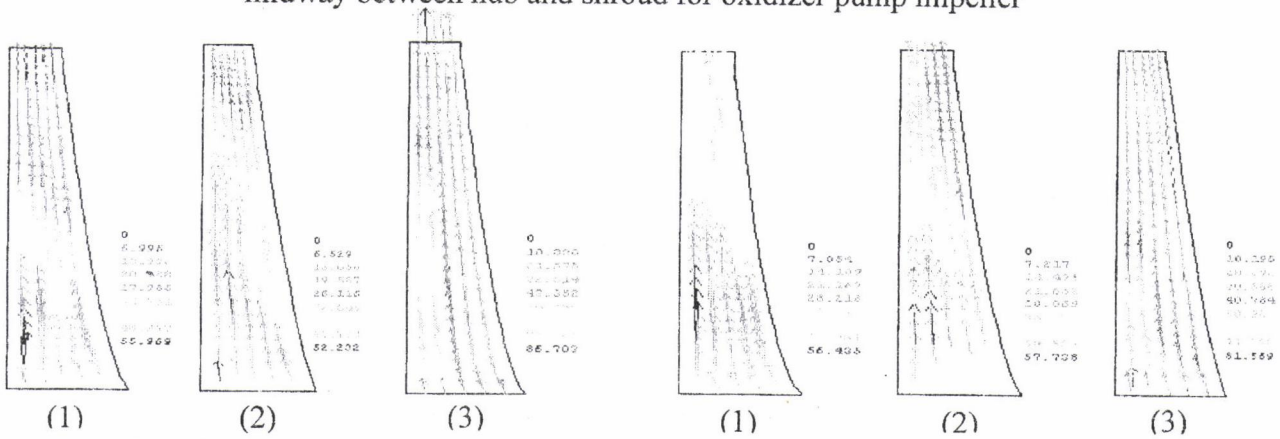

a) At (Φ/Φ_m) = 0.6 b) At (Φ/Φ_m) = 1.0

Fig. (5.16) Flow velocity vector and value in (m/s) for hub-to-shroud surface of oxidizer pump

1. Near the suction side
2. At the midway of the passage
3. Near the pressure side

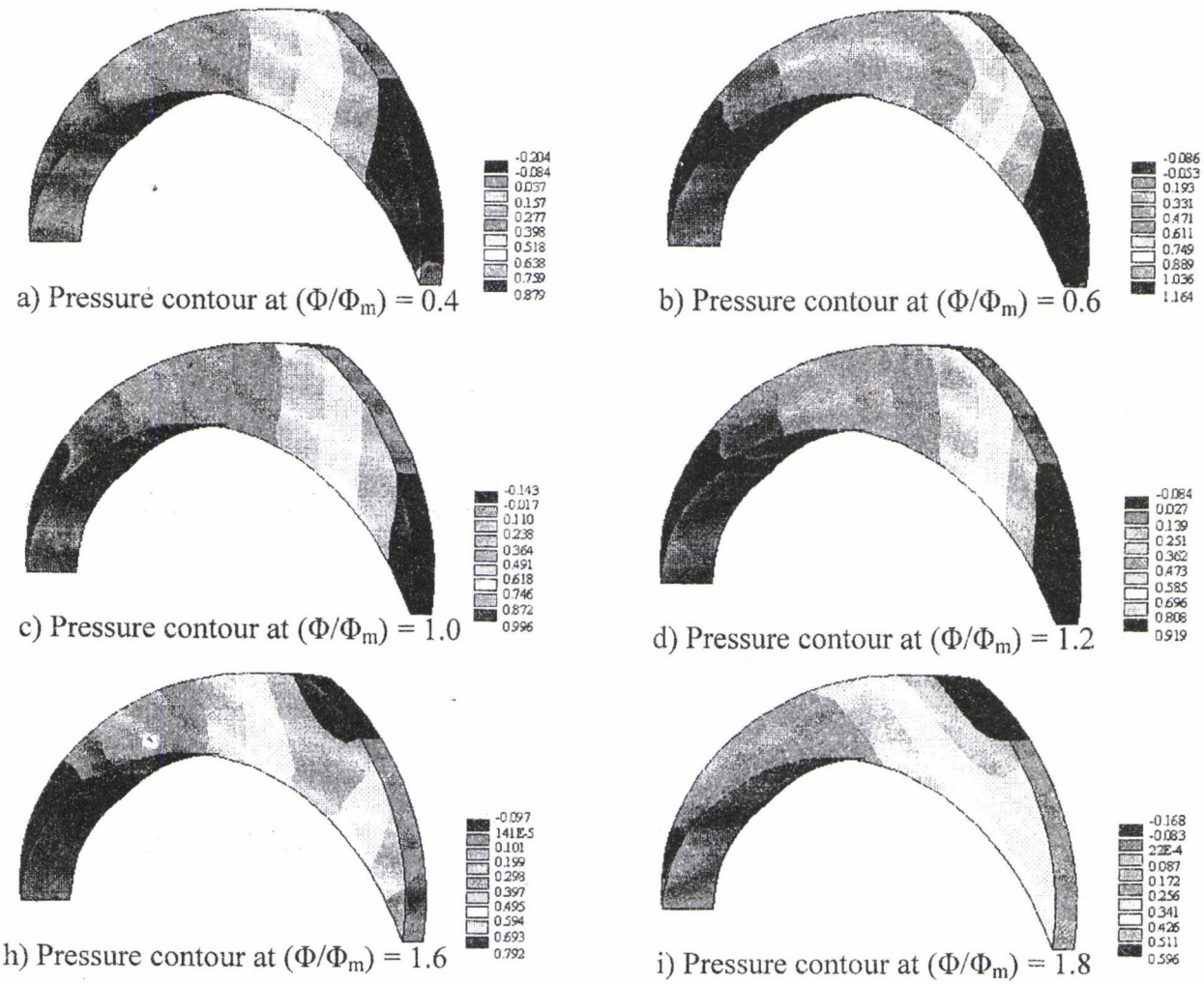

Fig. (5.17) Pressure contour on the blade-to-blade surface in the midway between hub and shroud for oxidizer pump impeller

The velocity distribution on the hub-to-shroud surface is represented in **Fig. (16a)** and **(b)** as a velocity vector. **Fig. (16a)** shows the velocity distribution when $(\Phi/\Phi_m) = 0.6$ at three positions. **Fig. (16a) (2)** represents the results at the midway of the passage and **Fig. (16a) (3)** represents the results near the pressure side. The flow velocity has a higher value near the hub than that near the shroud at the suction side as shown in **Fig. (16a) (1)**, and this difference in velocity is increased in **Fig. (16a) (2)** and has a significant value in **Fig. (16a) (3)**, which shows highest levels of velocity. **Fig. (16b)** represents the velocity distribution when $(\Phi/\Phi_m) = 1.0$ at the same three positions. The velocity distribution here has the same behavior with a remarked velocity reduction in the upper half of the passage as shown in **Fig. (16b) (1)**, and this reduction is increased after the suction side as seen in **Fig. (16b) (2)** and **Fig. (16b) (3)**, where the velocity has a lowest levels.

The pressure distribution in the impeller passage is represented by three dimensional pressure contours for a wide range of flow rate as shown in **Fig. (17)**. The general trend of the pressure distribution in the impeller passage for the all flow rate range is similar where the pressure increases with flow direction, but there are some differences in the pressure contour shape. When $(\Phi/\Phi_m)=0.4$, the inclination angle of the pressure contours with the circumferential direction near the suction side is less than that everywhere, and the pressure is reduced near the suction side with the possibility of cavitation occurring as shown in **Fig. (17a)**. When the flow rate is increased up to $(\Phi/\Phi_m)=0.6$, the pressure contours have no inclination with the circumferential direction near the

suction side where no pressure increasing toward the circumferential direction in this region as shown in **Fig. (17b)**. **Fig. (17c)** represents the results when (Φ/Φ_m)=1.0 where the pressure contour has a larger inclination angle than that at lower flow rates specially near the suction side and approximately the same manner is noticed in **Fig. (17d)** where (Φ/Φ_m)=1.2. A remarkable change is noticed in pressure distribution when (Φ/Φ_m)=1.6 especially near the passage exit where the pressure is reduced near the pressure side at the exit because of the high flow velocity resulted in this region as shown in **Fig. (17e)**. A similar pressure trend is occurred when (Φ/Φ_m)=1.8 with more reduction in pressure levels because of the high velocities resulted due to increasing the flow rate as shown in **Fig. (17f)**.

Another view for the pressure distribution in the impeller passage is presented by plotting pressure contour on the hub-to-shroud surface for two flow rates as shown in **Fig. (18a)** and **(b)**. The general trend for the pressure distribution in these figures is approximately unique as observed in Murakami impeller where the pressure is distributed uniformly except in the inlet region where the flow has just been turned from axial to radial direction and this causes a disturbance in flow characteristics.

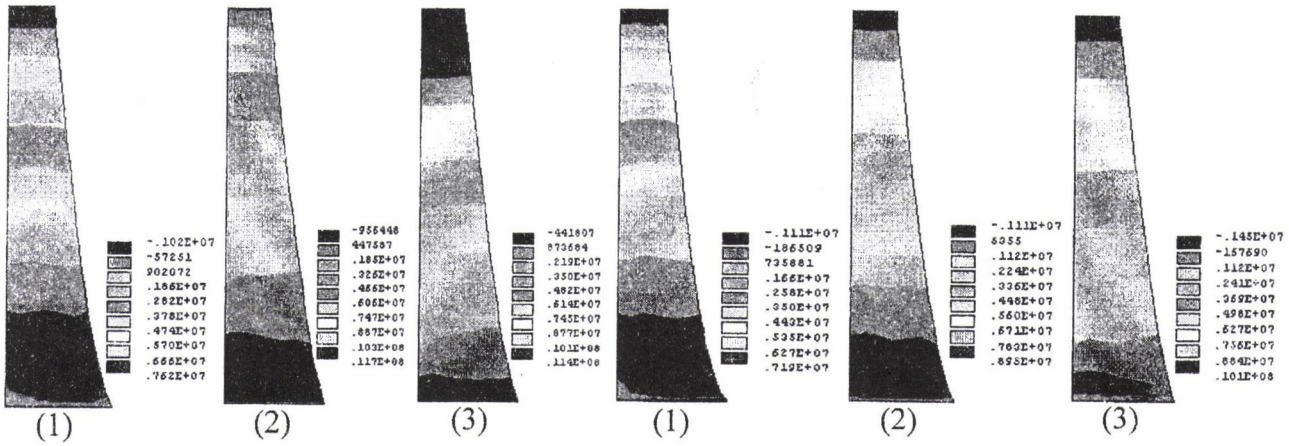

a) At (Φ/Φ_m) = 0.6 b) At (Φ/Φ_m) = 1.0

Fig. (5.18) Pressure contour for hub-to-shroud surface of oxidizer pump

1. Near the suction side
2. At the midway of the passage
3. Near the pressure side

Characteristic Curve of Oxidizer Turbopump Impeller

The all previous analysis work has been done to obtain a description for the flow behavior inside the impeller passage designed by the present method. Another impetus made the design work tends to the analysis work is to obtain the head characteristic curve, which represents the relation between the pressure head delivered and the flow rate. The characteristic curve of the oxidizer impeller resulted by the present analysis work is shown in **Fig. (19)**. The general trend of this curve refer to the increasing in flow rate cause a reduction in the pressure head delivered and this result is realistic for this kind of pumps where the outlet blade angle is less than 90 degrees. Although there is unsteady behavior near the shut-off capacity, but a wide rang of capacity has steady operation condition before and after the design point. The operation condition is far from the unsteady region and the pump operates in the safe region where the possibility of surging is slightly occurring and this represents very good characteristics for a new theoretical design pump.

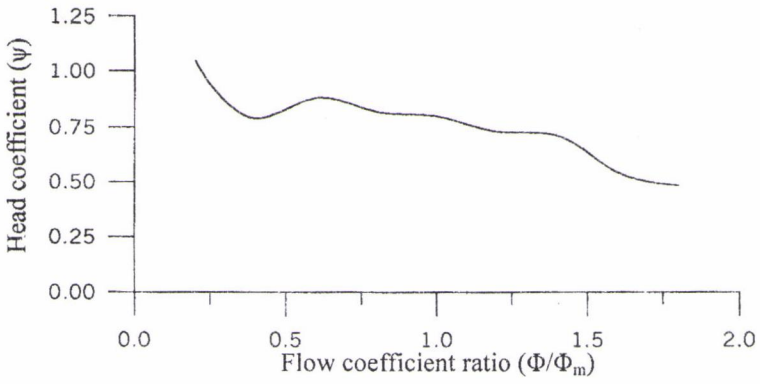

Fig. (19) Characteristic curve of high-speed oxidizer pump impeller

REFERENCES

Abu-Tabikh, M. I., (1990), The Utilization of Turbulence Model in Fluid Flow Calculation Through Turbomachines.

Al-Hamdani, S. H., (1993), Computer Method for The Design of a Centrifugal Pump Impeller.

Dixon, S. L., (1975), Fluid Mechanics Thermodynamics of Turbomachinery.

Huzel, D. K., Huang, D. H., (1967), Design of a liquid propellant rocket engines.

Lorett, J.A. and Gopalakrishnan, S., (1986), Interaction Between Impeller and Volute of Pumps at Off-Design Conditions.

Murakami, M., Kikuyama, K. and Asakura, E., (1980), Velocity and Pressure Distributions in the Impeller Passages of Centrifugal Pumps.

Salisbury, A. G., (1983), Current Concepts in Centrifugal Pump Hydraulic Design.

Sheet, H. E., (1950), The Flow Through Centrifugal Compressors and Pumps.

Stepanoff, A.J., (1957), Centrifugal and Axial Flow Pumps.

Wiesner, F. J., (1967), A Review of Slip Factors for Centrifugal Impellers.

NOMENCLATURE

Latin Symbols

A Cross sectional area of the flow.
b Blade width.
D Diameter.
f Friction factor.
g Acceleration of gravity.
H Head of liquid in the delivery tube.

L	Meridional blade length.
L_n	Length of nozzle.
l_m	Mixing length.
N	Rotational speed of impeller.
n	Blade number.
P	Pressure.
Q	Volumetric flow rate.
R	Radius coordinate.
r_c	Radius of streamline curvature.
s	Distance along quasi-orthogonal.
t	Blade thickness.
U	Blade velocity.
V	Absolute velocity.
W	Relative velocity.
y	Distance to the nearest point to the wall.
z	Axial coordinate.

Greek Symbols

α	Angle between meridional streamline and z-axis.
β	Angle between relative velocity and meridional plane.
β'	Blade angle.
ϕ	Angular coordinate.
ϕv	Volute angle.
ω	Angular velocity of the impeller.
ψ	Angle between the normal to the quasi-orthogonal and z-axis.
Φ	Flow coefficient.
Ψ	Pressure head coefficient.
μ_{eff}	Effective viscosity.
$\mu_{turbulent}$	Turbulent viscosity.
λ	Angle of nozzle divergence.
γ	Angle between the sides of volute walls.
ξ	Angle between two blades.

Subscript

1	Blade inlet.
2	Blade outlet.
e	Impeller eye.
f	Relative to the mean stream surface.
h	Hub.
L	Leakage.
m	Meridional component.
n	Normal.
noz	Nozzle.
s	Shroud.
T	Total.
t	Throat.
v	Vapor.
z	Axial component.
ϕ	Tangential component.
$z\phi$,$r\phi$,rz	Shear stress components.

Abbreviations

PS	Pressure side
SS	Suction side